J. Space Weather Space Clim. 2022, **12**, 38

https://doi.org/10.1051/swsc/2022035

JSWSC

Available online at:
www.swsc-journal.org

RESEARCH ARTICLE OPEN ACCESS

On the global ionospheric diurnal double maxima based on GPS vertical total electron content

Peng Chen[1,2,3,*], Rong Wang[1], Yibin Yao[4,5], Zhiyuan An[1], and Zhihao Wang[1]

[1] College of Geomatics, Xi'an University of Science and Technology, Xi'an 710054, China
[2] State Key Laboratory of Geodesy and Earth's Dynamics, Innovation Academy for Precision Measurement Science and Technology, CAS, Wuhan 430077, China
[3] Beijing Key Laboratory of Urban Spatial Information Engineering, Beijing 100045, China
[4] School of Geodesy and Geomatics, Wuhan University, Wuhan 430079, China
[5] Key Laboratory of Geospace Environment and Geodesy, Ministry of Education, Wuhan University, Wuhan 430079, China

Received 16 January 2022 / Accepted 21 October 2022

Abstract – Ionospheric diurnal double maxima (DDM) is a twin-peak pattern in the ionospheric electron density/total electron content (TEC) during the daytime. Understanding the characteristics of DDM is essential to study the physical mechanisms of the ionosphere. In this paper, the vertical TEC data (VTEC) in 2019–2020 derived from 537 globally distributed GPS stations were used to investigate the DDM phenomenon. The results reveal that the occurrence rate of DDMs is roughly quasi-symmetrical about the magnetic equator. In the northern hemisphere, it first increases, then decreases, and finally increases with the increase of magnetic latitude. The DDM phenomenon also exhibits significant seasonal variation. It mainly appears in summer/winter in the northern/southern hemisphere, and the valley and the second peak usually appear earlier in winter and later in summer. According to the difference in the magnitude of the two peaks of DDM, the DDM phenomenon is mainly manifested as the front peak significant type or the posterior peak significant type. The probability of the former shows an M-shaped variation with increasing longitude in the middle and high latitudes of the northern hemisphere and an inverted V-shaped variation in the high latitudes of the southern hemisphere within 180°W~60°W. The probability of the posterior peak significant type shows a trend opposite to the front peak significant type in each area. The occurrence time of DDM structures is usually about one hour later in low-latitude regions than in other regions, and the duration is usually shorter than in other regions. The relative magnitude of the DDM's twin peaks in low-latitude regions is usually smaller than in other regions.

Keywords: Diurnal Double Maxima / GPS / VTEC / Occurrence rate

1 Introduction

Under the influence of solar irradiation, the ionospheric electron density in the middle and low latitudes usually shows a diurnal variation, reaching the maximum around noon and a low value at night (Wang et al., 2021). However, due to the influence of dynamic processes such as $E \times B$ drift and neutral winds, the electron density/total electron content (TEC) sometimes decreases at noon and reaches its peak in the morning and afternoon, showing a twin-peak structure (Rajaram, 1977). Previous research suggested that this may be a brief depletion period of ionization during the peak followed by a recovery, thus the phenomenon was called a "bite-out" (Katamzi, 2011). However, follow-up studies showed that in addition to the "bite-out", the double peaks also appear with an additional plasma enhancement prior to or after the midday peak (Katamzi, 2011). To incorporate the different types of double peak structures, Pi et al. (1993) named these phenomena diurnal double maxima (DDM). We keep using this definition hereafter without other specifications.

Observations of the DDMs at different latitudes have been reported as early as the 1960s (Katamzi et al., 2016). Kohl et al. (1968) observed the DDM phenomenon at different latitudes and found that it is strongest in summer. The DDMs occur not only in the regions close to the peak of the equatorial anomaly, but also in the high latitude regions with a magnetic latitude (MLAT) as high as 40°N or higher, and the initial time of DDMs also varies with latitude (Huang & Jeng, 1978). The occurrence of the DDMs traveling from a higher latitude to a lower one is maximum in winter and minimum in summer,

*Corresponding author: chenpeng0123@gmail.com

and a reversed seasonal trend was observed for the bite-outs which traveled from lower to higher latitudes (Khan et al., 1985). Saryo et al. (1989) found that the DDM phenomenon moved from high to low latitudes and showed that poleward neutral winds might cause this. Adeniyi and Joshua (2014) presented that the occurrence rate of DDMs may decrease with increasing latitude. Katamzi et al. (2016) showed that the DDM structures (two peaks and one valley) in the southern hemisphere appeared earlier than in the northern hemisphere and the DDM structures not only propagated to the equator but also propagated to the polar direction. The ionospheric DDMs have an obvious seasonal correlation, and the seasonal extension of DDMs in low latitudes seems to be larger than at higher latitudes (Chen et al., 2021).

Although different data and methods have been used to study the phenomenon of DDMs in the ionosphere (e.g., Lee, 2012; Opio et al., 2015; Joshua et al., 2018; Chen et al., 2020; Jonah et al., 2020), the characteristics of DDMs have not been fully investigated. Zhang et al. (2000) used the MU radar in Japan to study the DDM event and showed that forenoon DDMs only appear in summer instead of other seasons. However, Katamzi et al. (2012) found that the forenoon DDM event happens in Italy's autumn. Huang and Jeng (1978) used the foF2 data of Chung-li (24.95°N, 121.23°E) to study the DDM phenomenon and showed that the DDM phenomenon could be observed in the MLAT of 40°N or even higher latitudes. However, Adeniyi and Joshua (2014) showed that in the NmF2 and hmF2 data, it is difficult to observe the DDM phenomenon beyond the MLAT of 21.77°N. Pavan Chaitanya et al. (2015) studied the variations of foF2 at low latitudes in India. Their results showed that the ionospheric DDMs are more apparent in equinoxes than in other seasons. In the study of NmF2 in Africa's magnetic equatorial region, Adebesin et al. (2018) found that the DDMs in the southern hemisphere occurred 1–2 h later in the June solstice (local winter) than in other seasons. Chen et al. (2021) studied DDMs using foF2 data in East Asia, and the results showed that DDMs in the northern hemisphere mainly occur in summer (May–August), and lower latitude regions can extend to September. However, an opposite result was found by Wang et al. (2021) using the BDS geostationary (GEO) satellite vertical total electron content (VTEC) in the Asian-Australian area. It showed that DDMs mainly appear in the summer and winter in the northern hemisphere and summer in the southern hemisphere. In addition, DDMs occur slightly earlier in the local winter than in the local summer. As the findings of DDMs derived from different data, methods, and regions are not consistent, further studies to investigate the characteristics of DDMs are still needed.

In previous studies, the characteristics of DDMs observed in different regions and under different conditions may not be consistent. At present, global navigation satellite systems (GNSS) technology has become a hot spot in the field of ionospheric research. GNSS tracking stations cover most of the world's land and part of the ocean. Through a large number of ground observation stations, all-weather monitoring of the ionosphere can be achieved. Previously, some studies have observed the ionospheric DDM event in GNSS TEC and used GNSS TEC to study it (Mukherjee et al., 2010; Ouattara et al., 2012; Katamzi et al., 2016; Venkatesh et al., 2016; Oluwadare et al., 2019; Huang et al., 2020; Wang et al., 2021). Ouattara et al. (2012) observed that the two peaks of the DDM phenomenon in global positioning system (GPS) TEC profiles mainly occur in the morning/afternoon and evening. Katamzi et al. (2016) used GPS TEC to study the DDM phenomenon in southern African and European middle-latitude regions, and the results showed that the DDM phenomenon occurs earlier in the southern hemisphere than in the northern hemisphere and shows an equatorward tendency in both hemispheres. Wang et al. (2021) used BDS GEO VTEC to study DDM phenomena in the Asian-Australian area and found that the DDM phenomena have latitudinal, seasonal, and hemispheric differences.

However, previous research on DDMs was limited to the studied area and the insufficient number of stations. Furthermore, many studies focused on the latitudinal variations of the DDM phenomenon, while the longitudinal variations have not been fully investigated. Earlier studies have shown that the magnitude of the two peaks of a DDM event has an obvious longitude dependence (Anderson, 1973; Rajaram, 1977; Bhuyan & Borah, 2007), while the selected study area is still relatively small, and it is not easy to reflect the variations in a larger area. Therefore, this paper uses GPS observations from 537 GNSS tracking stations worldwide to investigate the DDM phenomena on a global scale accounting for their regional differences. The characteristics of the DDM phenomenon are statistically investigated from four aspects: the occurrence rate of DDMs, the comparison of the magnitude of the two peaks, the occurrence time and duration of the DDM structures, and the relative magnitude of the two peaks.

This paper is organized as follows. Section 2 introduces the method and data used to calculate the GPS VTEC. Section 3 investigates the characteristics of DDMs from different aspects. Section 4 discusses the possible physical mechanisms behind the DDM characteristics. Finally, the conclusions are given in the Section 5.

2 Method and data

2.1 The calculation of GPS VTEC

GPS has the advantages of wide coverage and all weather. Therefore, this paper uses GPS VTEC to study the daytime DDM structures. The GPS VTEC results of each station are calculated using the IONOLAB-TEC software developed by the IONOLAB Group (Arikan et al., 2003, 2004, 2008; Nayir et al., 2007; Sezen et al., 2013). The IONOLAB-TEC software contains the IONOLAB-BIAS algorithm, which can solve the receiver differential code bias (RDCB) using the global ionospheric maps (GIMs), carrier phase smoothing pseudo-range observations, satellite differential code bias (SDCB) and ephemeris data (Arikan et al., 2008). The VTEC values with 30 s time resolution are then computed using dual-frequency pseudo-range observations/carrier phase smoothing pseudo-range observations, SDCB, and RDCB for all receiver locations (Arikan et al., 2003, 2004). Finally, a regularized estimation algorithm is used to combine the VTEC calculated from all available satellites to make a reliable estimate of the TEC in the zenith direction of the GPS receiver. (Erol et al., 2002; Arikan et al., 2003, 2004, 2007, 2008; Nayir et al., 2007; Sezen et al., 2013). Table 1 shows the data and the main parameter settings for calculating GPS VTEC using IONOLAB-TEC.

Table 1. Primary data sources and data processing strategies of IONOLAB-TEC.

Data/parameter	Format/types	Source/strategies
GPS dual-frequency observations	RINEX	IGS MGEX, UNAVCO, IBGE
GIMs	IONEX	CODE
DCBs		CODE
Precise ephemeris		CODE
Observable types	C1/P1, P2, L1, L2	Regularized estimation
Mapping function (MF)	Single layer MF	Ionospheric shell height: 428.8 km
Cutoff elevation angle		10°

The VTEC calculated in this way has good precision in both the ionosphere quiet and disturbed periods and is in good agreement with the results of the IGS (International GNSS Service) analysis center. It also has certain advantages in representing and tracking sudden temporal variations of the ionosphere (Erol et al., June, 2002; Arikan et al., 2003, 2004; Nayir et al., 2007). In addition, the results are highly accurate in detecting disturbances and irregularities for various time scales and stations (Arikan et al., 2007).

2.2 Data

This paper selects the GPS observations of 537 GNSS tracking stations worldwide from 2019 to 2020 to study the global DDM phenomenon, as shown in Figure 1. Among them, the data for most of the stations (387 stations) comes from the IGS Multi-GNSS Experiment (MGEX) network (blue triangles), the data for 25 stations in Brazil comes from Instituto Brasileiro de Geografia e Estatística (IBGE, golden diamonds), and the data for the remaining 125 stations comes from UNAVCO (magenta squares). One can see from this figure that GNSS tracking stations are well-distributed over the globe, covering most of the land and part of the ocean.

This paper defines the DDM phenomenon in GPS VTEC as follows:

1. DDM phenomenon must occur during the local daytime (after sunrise and before sunset, LT = UT + lon/15).
2. The two peaks of a DDM must be greater than the average value of TEC within the day.
3. The ratio of the difference between each peak and the valley to its peak must be greater than 0.03.
4. The ratio of the smaller peak-to-valley difference to the larger peak-to-valley difference needs to be greater than 0.14.
5. The time interval between two peaks should be greater than 75 min.

Among them, condition 2 aims to remove the impact of the ionospheric irregular disturbance on the identification of double peaks as much as possible. Conditions 3 and 4 are based on our previous study of the peak size of DDMs (Wang et al., 2022). Condition 5 is to avoid the influence of short-period ionospheric fluctuations, such as medium-scale traveling ionospheric disturbances (Wang et al., 2021). An ionospheric DDM event was considered to be detected if all the above conditions were fulfilled.

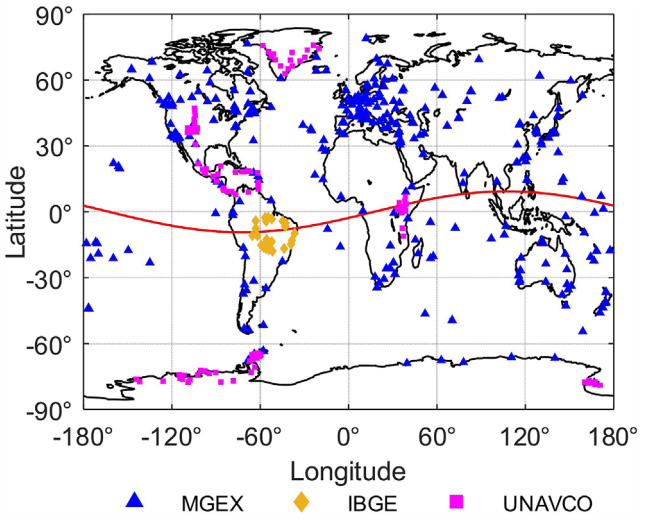

Figure 1. Distribution of GNSS stations used in this study. The blue triangle in the figure represents the IGS MGEX stations, the yellow diamond represents the IBGE stations, and the magenta square represents the UNAVCO stations. The solid red line represents the magnetic equator.

Figure 2 shows the normal VTEC variations and the VTEC variations with the DDM phenomenon of DOY (day of the year) 254 in 2020. Among them, the AREG has a normal variation, while the YKRO, SEME, and DARW have obvious DDM phenomena (one valley sandwiched by two peaks). In order to distinguish between these two peaks, the first peak will be referred to as peak1, and the second peak will be referred to as peak2 in the following.

3 Statistical results

To better understand the characteristics of DDMs, we analyze statistically the variation of the DDMs on a global scale from four perspectives: the occurrence rate of DDMs, the comparison of the magnitude of two peaks, the occurrence time and duration of the DDM structures, and the relative magnitude of each peak.

3.1 The occurrence rate of DDMs

Figure 3 shows the occurrence rate of the DDM phenomenon at each station in 2019–2020. The occurrence rate

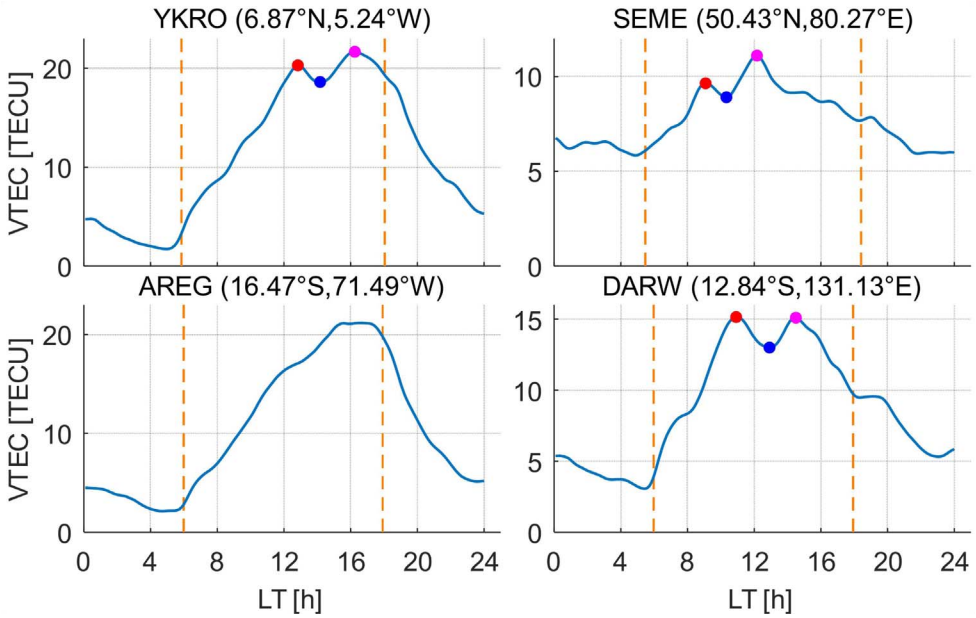

Figure 2. Diurnal VTEC variation shows a DDM phenomenon and no DDM phenomenon in DOY 254 in 2020. The coordinates in the figure are the geographic coordinates of each station. Peak1, valley, and peak2 of the DDMs are marked in red, blue, and magenta, respectively. The orange vertical dotted lines represent the local sunrise and sunset time.

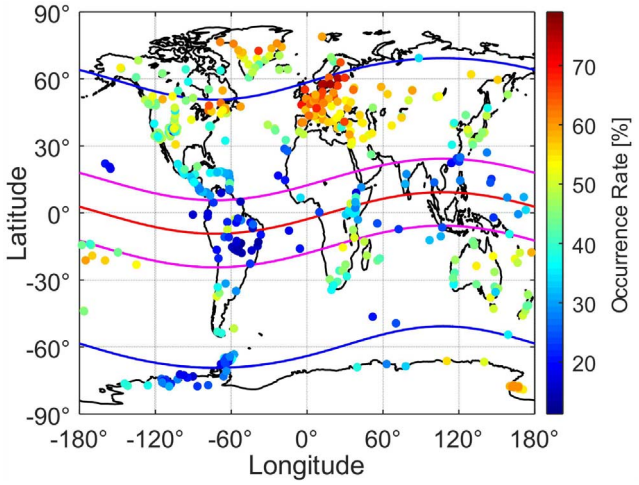

Figure 3. The occurrence rate of the DDM phenomenon observed at each station during 2019–2020. In the figure, the solid red line represents the magnetic equator, the solid magenta line represents the MLAT ±15°, and the solid blue line represents the MLAT ±60°.

of DDMs in the figure is obtained by dividing the number of days with the DDM phenomenon by the total number of days of data. In Figure 3, we found that the occurrence rate of DDMs shows a significant latitudinal difference. In general, the average occurrence rate in low-latitude regions ($-15° < \text{MLAT} < 15°$) is ~25%, significantly lower than in mid/high-latitude regions. Stations with a DDM occurrence rate greater than 60% are mainly located in Europe, eastern North America, Greenland, and eastern Antarctica. In addition, around the MLAT ±60°, the occurrence rate of DDMs is lower than that of adjacent latitudes. This is particularly obvious in Canada in northern North America, where the occurrence rate of DDMs is lower than that of the United States in the south and Greenland in the north. This phenomenon also exists near the MLAT of −60° in the southern hemisphere but is not as obvious as in the northern hemisphere due to the small number of tracking stations. In addition, the occurrence rate of DDMs also shows a significant difference in longitude. This is very obvious in North America, Eurasia, and Antarctica. The occurrence rate of DDMs on the Atlantic coast of the northern hemisphere is higher than that on the Pacific coast, while in the east of Antarctica, it is higher than in the west.

In order to reflect the variation of the occurrence rate of DDMs with latitude more intuitively, Figure 4 shows the variation of the occurrence rate of DDMs at each station with the MLAT. In general, the occurrence rate of DDMs is mainly concentrated in the range of 13–75%, and it exhibits a quasi-symmetrical distribution on both sides of the magnetic equator. In the northern/southern hemispheres, with the decrease/ increase of MLAT, it first decreases, then increases, and finally decreases. In the range of MLAT 0°~47°, with the decrease of MLAT, the occurrence rate of DDMs decreases from ~75% to ~13%, and finally, a valley occurs near the magnetic equator. While in the range of MLAT 47°~80°/−45°~−80°, the occurrence rate of DDMs first decreases and then increases with the decrease/increase of MLAT, and a valley appears near 72°/65°. In the range of 47°~80° of MLAT, the occurrence rate of DDMs decreases from ~75% to ~38% and then increases to ~60%. In the range of −40°~−80° of MLAT, the occurrence rate of DDMs decreases from ~45% to ~16% and then increases to ~61%. The occurrence rate of DDMs in the MLAT range of 40°~60° in the southern hemisphere is slightly lower than that in the northern hemisphere at the same latitude. Interestingly, with the increase of MLAT, the decreasing/increasing area of DDM occurrence rate in the northern/southern hemispheres is mainly

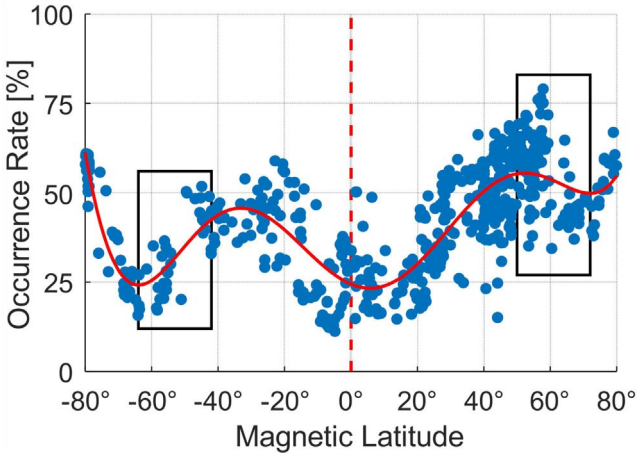

Figure 4. The variation of the occurrence rate of DDMs at each station with its magnetic latitude. The red dotted line in the figure represents the magnetic equator. The solid red line is the trendline obtained by polynomial fitting to each point in the figure. The black rectangle represents the area where the occurrence rate of DDMs in the northern/southern hemisphere shows a downward/upward trend as the magnetic latitude increases.

located in the mid-latitude trough areas of each hemisphere. Some studies have shown that the mid-latitude trough is mainly located between 45° and 70° of MLAT (e.g., Liu et al., 2015; He et al., 2020). During the magnetic quiet period, the center of the mid-latitude trough is located near the corrected magnetic coordinates ±60° (Yang et al., 2015), which is very close to the valley of the DDM occurrence rate in this area. Although ionospheric mid-latitude trough/main trough mainly occurs at night, this phenomenon can also be observed during the daytime (e.g., Moffett and Quegan, 1983; Pryse et al., 1998; Karpachev et al., 2019), which is particularly obvious in the southern hemisphere (Horvath & Essex, 2003). Therefore, whether the downward trend of the occurrence rate of DDMs in this region is related to the mid-latitude trough requires more in-depth research in the future.

Previously, some studies showed that ionospheric DDMs usually occurred under low background electron density/TEC conditions (Zhang et al., 2000; Wang et al., 2021) and suggested that the low background TEC (averaged daytime VTEC) may be the precondition for the generation of ionospheric DDMs (Wang et al., 2021). Therefore, the stations were grouped into different regions for each hemisphere to investigate the relationship between background TEC and the occurrence rate of DDMs. The regions were defined according to the variation trend of the occurrence rate of DDMs with MLAT. Figure 5 shows the variation of the occurrence rate of DDMs with the background VTEC in different seasons in each region. In the figure, the occurrence rate of DDMs at each station in each season is obtained by dividing the number of days with DDMs in the season by the total number of days in the season. The background VTEC at each station is the seasonal daytime average VTEC. The seasons in the figure have been classified as local seasons in their respective hemispheres (December–February, March–May, June–August, and September–November are winter/summer, spring/autumn, summer/winter, and autumn/spring in the northern/southern hemisphere, respectively). For example, data in Jan 2019, Feb 2019, Dec 2019, Jan 2020, Feb 2020, and Dec 2020 were used for the northern hemisphere winter. Other seasons are similar to winter, with six months of data for each season. In Figure 5, it can be found that the occurrence rate of DDMs in the range of 0–45° of MLAT in both hemispheres is negatively correlated with the background VTEC, i.e., shows a clear downward trend with the increase of the background VTEC. In addition, the occurrence rate of DDMs shows some seasonal differences. This is particularly evident in the range of MLAT 45°N~70°N, where the occurrence rate of DDMs seems to increase with the increase of background VTEC, and it is significantly higher in summer and spring than in winter. The region where the MLAT of the northern/southern hemisphere is greater than 70° shows a similar trend, but more clearly.

Figure 6 shows the occurrence rate of DDMs in different months at each station. It can be seen from the figure that the occurrence rate of DDMs shows obvious regional differences and seasonal variations. The DDM phenomenon in North America mainly appears in June–July, while in Central America, it mainly occurs in November–January, and in Greenland, it mainly occurs in May–August. In Europe, it mainly occurs in March–September, and in Asia, it mainly occurs in June–August. It varies relatively little within a year in South America but is still slightly higher in June–August than in other months. In Africa, the occurrence rate of DDMs in May–August is significantly higher than in other months, while the ionospheric DDMs in Australia mainly occur in April–August and October–November. The occurrence rate of DDMs in mid/high latitudes varies significantly with the seasons. Europe's average occurrence rate exceeds 70% in April and July and only ~42% in December. In addition, the variation of the occurrence rate of DDMs in different regions of the world with the longitude and latitude shows different regularities in detail in each season. Overall, the seasonal variations in the occurrence rate of DDMs in the northern hemisphere are more obvious than in the southern hemisphere. The occurrence rate of DDMs on the Atlantic coast of the northern hemisphere is greater than that on the Pacific coast for most of the time, except in summer.

3.2 Comparison of the magnitude of the DDM's two peaks

In this paper, the DDM phenomenon is divided into three types according to the magnitude of the two peaks of the DDM structures, namely: the front peak significant type (peak1 > peak2), the two-peak equivalent type (peak1 ≈ peak2), and the posterior peak significant type (peak1 < peak2). The types are defined as follows:

See the equation (1) *bottom of the page*

$$\text{ratio} = \frac{\text{VTEC}_{\text{smaller peak}} - \text{VTEC}_{\text{valley}}}{\text{VTEC}_{\text{larger peak}} - \text{VTEC}_{\text{valley}}} \begin{cases} \text{if } \text{VTEC}_{\text{peak1}} > \text{VTEC}_{\text{peak2}} \text{ and ratio} < 0.9 \Longrightarrow \text{peak1} > \text{peak2} \\ \text{if } \text{VTEC}_{\text{peak1}} = \text{VTEC}_{\text{peak2}} \text{ or } \text{ ratio} \geq 0.9 \Longrightarrow \text{peak1} \approx \text{peak2} \\ \text{if } \text{VTEC}_{\text{peak1}} < \text{VTEC}_{\text{peak2}} \text{ and ratio} < 0.9 \Longrightarrow \text{peak1} < \text{peak2} \end{cases} \quad (1)$$

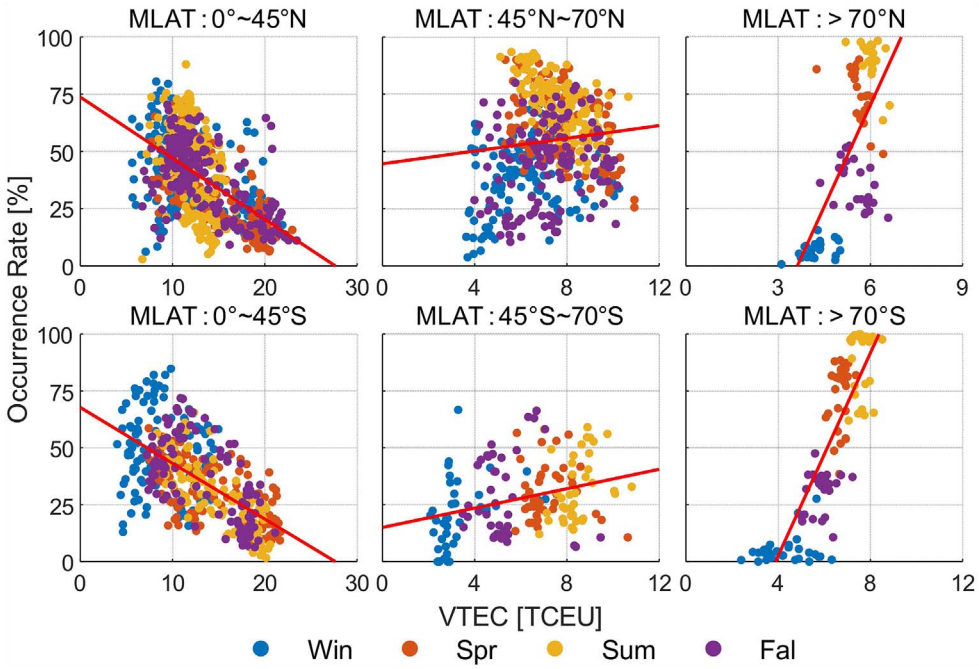

Figure 5. The variation of the DDM occurrence rate of each station in each season in different magnetic latitude areas with its background VTEC. In the figure, MLAT represents the magnetic latitude, and the solid red line results from the first-order linear fitting of each point.

where $VTEC_{smaller\ peak}$ represents the VTEC of the smaller peak of the two peaks; $VTEC_{larger\ peak}$ represents the VTEC of the larger peak of the two peaks; $VTEC_{valley}$ represents the VTEC of the valley.

Figure 7 presents the probability of various types of DDMs in the DDM phenomenon. The probability in the figure is obtained by dividing the number of days of each type of DDMs by the total number of days of DDMs. In Figure 7, it can be found that the probability of each type of DDMs shows obvious latitude, longitude, and hemispheric differences. The ionospheric DDMs are mainly manifested as the front peak significant type or the posterior peak significant type globally, and the probability of a two-peak equivalent type is small (the probability of most stations is 5%~10%, only a few stations have a slightly higher probability, but the maximum does not exceed 20%). The distribution of stations with a higher probability of front/posterior peak significant type shows a certain regularity globally. The former is mainly located in Eurasia at 0–100°E, the east coast of Africa, the western part of North America, northern Greenland, and the eastern and western parts of Antarctica. The latter is mainly located on the east and west coasts of the Atlantic Ocean, including eastern parts of North America, central South America, central Antarctica, and the west coast of Africa.

In order to more intuitively reflect the variation of the probability of various types of DDMs with the longitude, this paper divides the stations into five different regions according to the difference of MLAT: the high MLAT area of the northern hemisphere (NH, MLAT > 45°N), the middle MLAT area of the northern hemisphere (NM, MLAT: 15°N~45°N), low MLAT area (LM, MLAT: 15°N~15°S), southern hemisphere middle MLAT area (SM, MLAT: 15°S~45°S) and southern hemisphere high MLAT area (SH, MLAT > 45°S). Figure 8 shows the variation of the probability of each type of DDMs in different regions with the longitude. It can be found that in the NH/NM, the probabilities of the front peak significant type are mainly concentrated in 25%~75%, and show an "M" shaped variation with the increase of longitude, with an increasing trend in the range of 150°W~120°W and 30°W~60°E, and a decreasing trend in the range of 120°W~30°W and 60°E~150°E. It reaches peak values (~65%) around 120°W and 60°E and a valley value (~25%) around 30°W. The probabilities in LM/SM have no obvious variations with the increasing longitude, fluctuating around 37%/40%. In the range of 180°W~60°W in the SH, it first increases and then decreases with the increase of longitude, reaching a peak value (~70%) near 140°W, and has no obvious variation in the range of 40°E~180°E. The probability of the two-peak equivalent type does not change significantly with the increase of longitude in each MLAT region. In each MLAT region, the probabilities of the posterior peak significant type show the opposite trend to the front peak significant type with the increase of longitude. It shows a "W" shape variation in the NH/NM, reaching valley values (~25%) near 120°W and 60°E, and a "V" shape in the range of 180°W–60°W in the SH, reaching the valley value (~25%) near 140°W.

3.3 The occurrence time and duration of DDM structures

Figure 9 shows the probability that the DDM structures occur in each period in different MLAT regions. Overall, the occurrence time of the DDM structures shows an apparent latitudinal difference. The DDM structures appear earlier in the middle and high latitudes and later in the low latitudes. The probability distributions of the occurrence time of peak1 and valley in each period in the NH/NM show a unimodal trend.

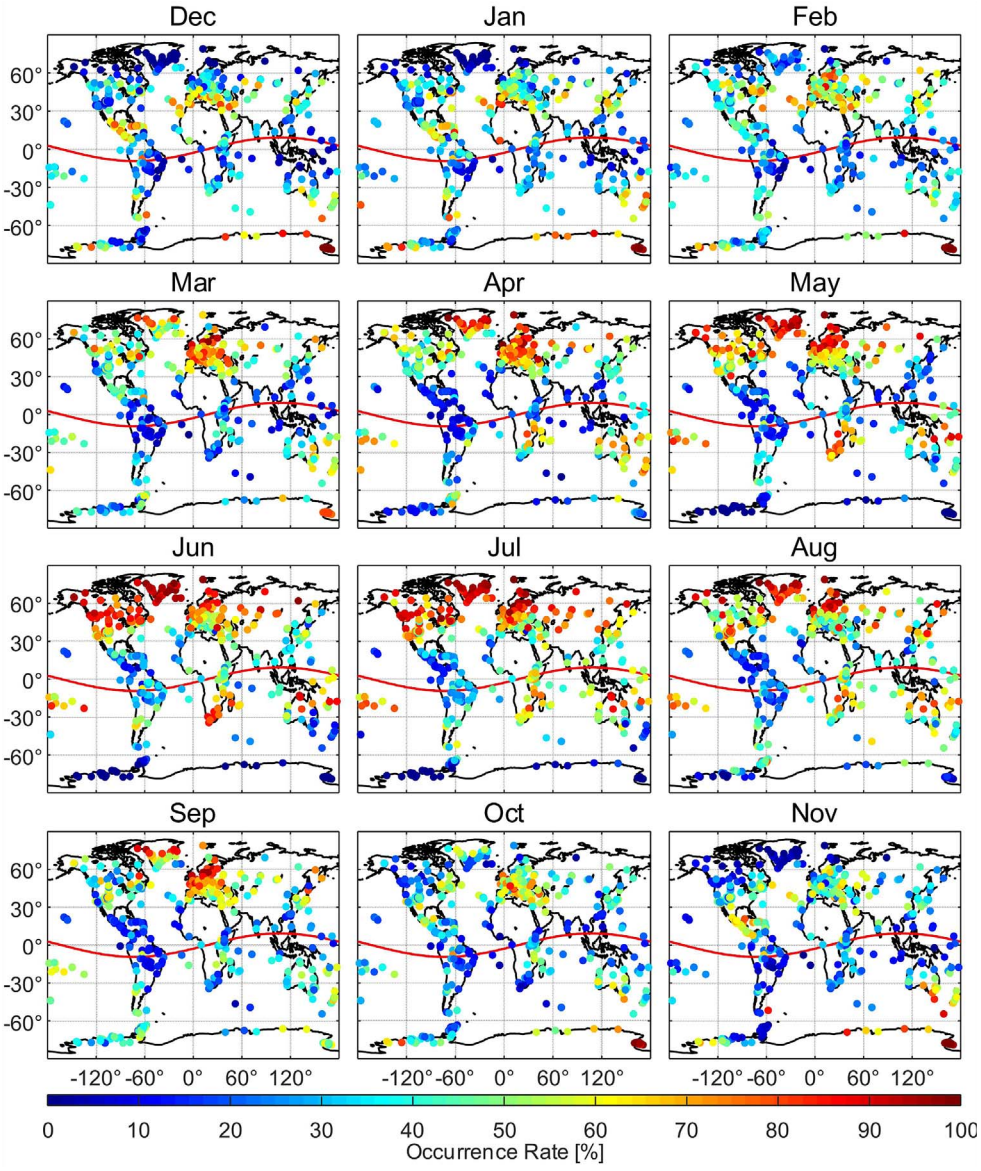

Figure 6. The occurrence rate of DDMs in each month at each station. The solid red line in the figure represents the magnetic equator.

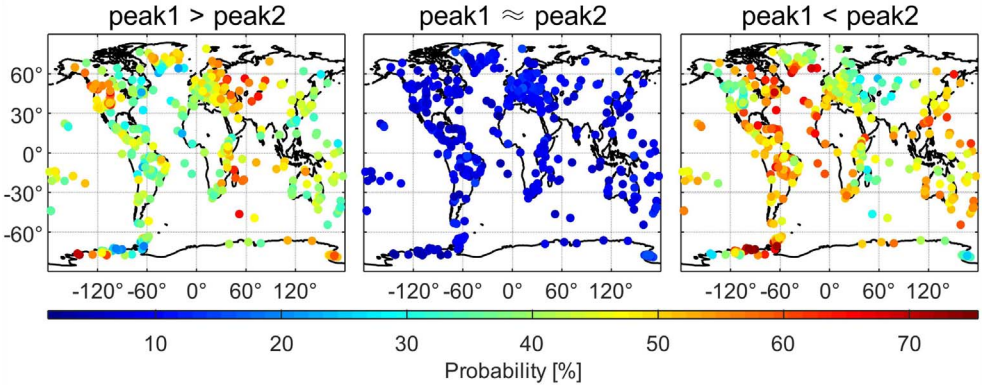

Figure 7. Comparison of the probability of different DDM types.

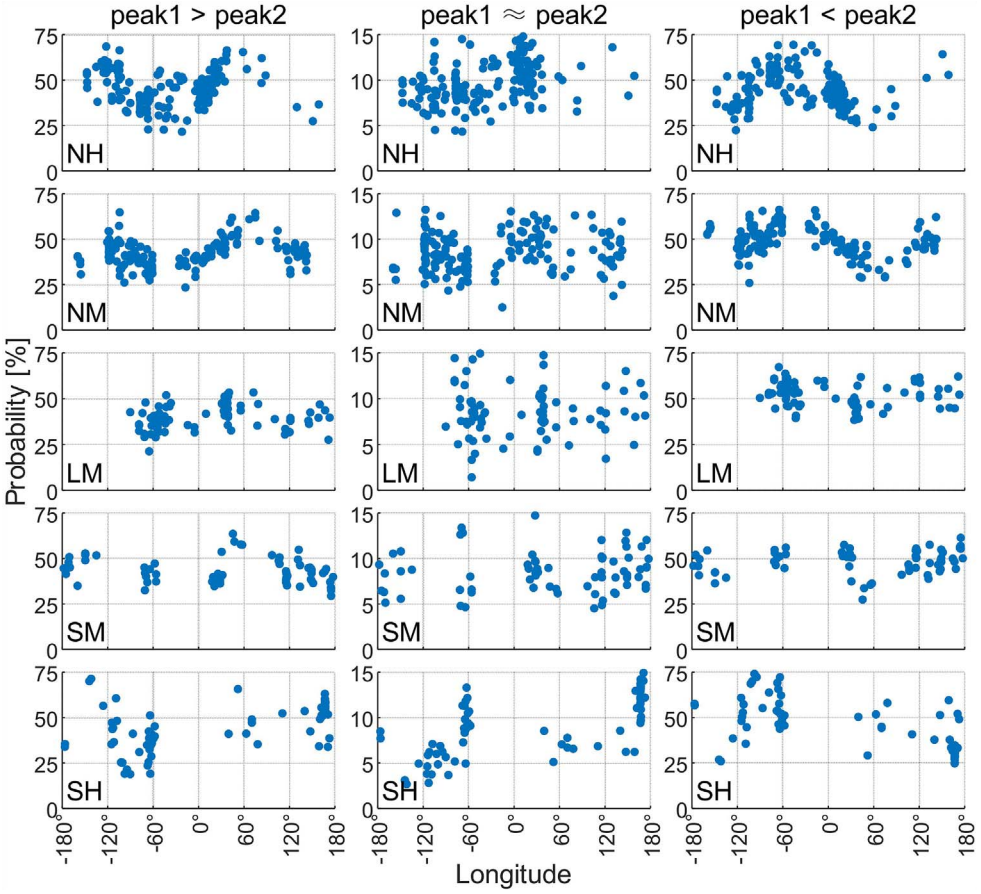

Figure 8. The variation of the comparison of the magnitude of the two peaks in different MLAT regions with the longitude.

Among them, peak1 of the DDM structures is more likely to fall between 10:00 and 13:00 LT, but most probably at 11:00–12:00 LT, the valley is more likely to fall between 12:00 and 15:00 LT, but most probably at 13:00–14:00 LT. Peak2 in the NH/NM is most likely to appear in 13:00–20:00 LT/13:00–19:00 LT. Peak1 in the LM region mainly occurs in 11:00–14:00 LT, valley mainly occurs in 13:00–16:00 LT, peak2 mainly occurs in 15:00–18:00 LT, and they are most likely to occur in 12:00–13:00 LT, 14:00–15:00 LT, 16:00–17:00 LT, respectively. Therefore, the occurrence time of DDM structures in LM is usually later than in the NH and NM. The probability of peak1 and valley appearing in the SM in each period shows a similar trend to that of the NM, both show a unimodal distribution, and the main occurrence time is also consistent with the NM. Peak1 in the SH mainly occurs in 9:00–12:00 LT, and peak2 mainly occurs in 12:00–20:00 LT. Peak2 is mostly likely to occur earlier in the SH region than in the NH region.

Figure 10 shows the duration of the DDM structures in different MLAT regions. The duration of the DDM structures in the figure is obtained by subtracting the LT when peak1 appears from the LT when peak2 appears. The duration of the DDM structures shows a similar trend in the LM, NM, and SM, but these trends are different from those in the NH and SH. The duration of DDMs is mainly concentrated in 2–6 h (NH: ~68.40%, NM: ~78.80%, LM: ~93.38%, SM: ~83.69%, SH: ~63.57%). The most likely duration of DDMs in the NM, LM, and SM regions is 3–4 h (NM: ~26.79%, LM: ~36.66%, SM: ~28.51%), while the duration in the NH and SH is the most likely within 2–4 h (NH: ~41.66%, SH: ~41.35%). The probability of DDM's duration in LM within 2–5 h (~84.21%) is significantly higher than in other regions (NH: ~54.49%, NM: ~63.98%, SM: ~67.88%, SH: ~54.10%), and the probability within 6–12 h (~4.49%) is significantly smaller. This means that the duration of the DDM structures in LM is usually shorter than in other regions. The duration of DDMs in the NH/NM is relatively close to that of the SH/SM.

Figure 11 shows the occurrence rate of DDM structures in different MLAT regions in different periods of each month. In Figure 11, we found that the occurrence rate of the DDM structures in each month and period shows obvious seasonal and latitudinal differences. Peak1 in the NH mainly occurs at 10:00–12:00 LT, among which, it mainly occurs at 11:00–12:00 LT in September–March (local autumn and winter) and 10:00–11:00 LT in April–August (local spring and summer), with the autumn and winter later than the spring and summer. Valley/peak2 mainly occurs at 12:00–15:00 LT/14:00–20:00 LT and shows an overall roughly inverted "U" shaped distribution as the month increases, with earlier occurrence time in the local winter and later occurrence time in the local summer. The main occurrence time of peak1 and valley in the NM are slightly different from those in the NH, and its variation with months is more pronounced than in the NH. The main occurrence time of valley and peak2 in this area also

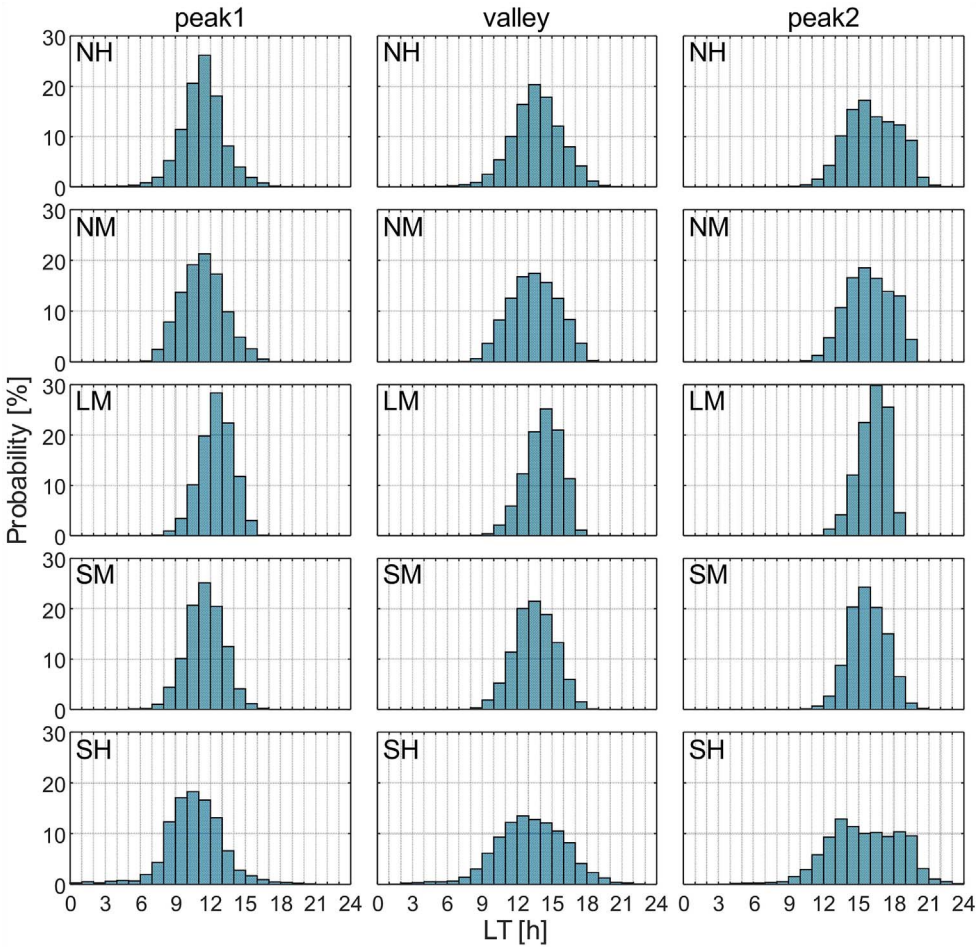

Figure 9. The histogram of the occurrence time of the ionospheric DDM structures in each MLAT region.

shows an inverted "U" shaped distribution with the increase of months, and it is more obvious than that of NH. The occurrence time of the DDM structures in LM varies relatively little with the month. Peak1, valley, and peak2 mainly appear in 12:00–13:00 LT, 14:00–15:00 LT, and 16:00–17:00 LT, respectively. The DDM structures in the SM mainly occur at 10:00-13:00 LT, 12:00–15:00 LT, and 14:00–18:00 LT, with an overall "U" shaped distribution as the month increases. The valley and peak2 in this region occur earlier in April–September (local autumn and winter) and later in October–March (local spring and summer). The occurrence time of the DDM structures in the SH varies more in each month, and the regularity of variations with the month is not as obvious as in other regions, but valley and peak2 still occur earlier in local winter than summer.

3.4 The relative magnitude of the DDM's two peaks

In order to more intuitively reflect the difference in the relative magnitude of each peak in latitude, Figure 12 shows the probability distribution of the relative magnitude of each peak in different MLAT regions. The calculation of the relative magnitude of each peak in the figure is as follows:

$$\text{relative magnitude}_{\text{peak}_i} = \frac{\text{VTEC}_{\text{peak}_i} - \text{VTEC}_{\text{valley}}}{\text{VTEC}_{\text{peak}_i}} \times 100 \quad (2)$$

where $\text{VTEC}_{\text{peak}_i}$ is the VTEC of the ith (i = 1 or 2) peak; $\text{VTEC}_{\text{valley}}$ is the VTEC of the valley.

It can be seen from the figure that the relative magnitude of the two peaks in the LM is mainly concentrated in 0–15%, while the relative magnitude in other regions is mainly concentrated in 5–20%, which means that the relative magnitudes of peak1 and peak2 in LM are usually smaller than those of other regions. The relative magnitude of each region has the highest probability in the range of 5–10%. The relative magnitudes of the two peaks in different MLAT regions show obvious differences. On a global scale, as the latitude decreases (getting closer to the equator), the probability of the relative magnitude of each peak in its main distribution range has a gradually increasing trend.

Figure 13 shows the probability distribution of the relative magnitude of the two peaks in different months in each MLAT region. It can be seen from the figure that the probability of the relative magnitude in the range of 5–10% shows a significant seasonal difference. The variation of the relative magnitude of peak2 with a month in the NM is similar to that in the NH, and the probability in May–August (local summer) is lower than in other seasons. The relative magnitude of peak1 in the NH has a lower probability in May–August (local summer), while in the NM, it has a lower probability in March (local spring) and June (local summer). In the LM, the relative magnitude of the

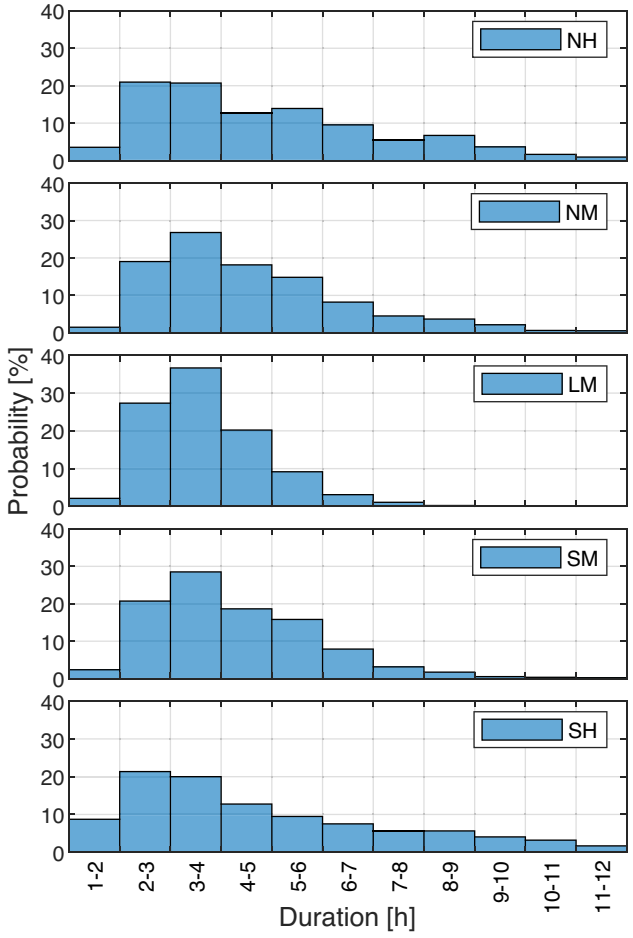

Figure 10. The duration of DDM structures in different MLAT regions.

peak1/peak2 has a higher probability in November–January, March, and July/November–December, February, and April than in other months. The probability of the relative magnitude of the two peaks in the SM in May and October is usually lower than that of other seasons, while the probability of the relative magnitude of the two peaks in the SH in November–March, June, and August is lower than that of other seasons.

4 Discussion

Most previous studies investigated the ionospheric DDM phenomenon by using a small number of stations and a relatively small area (e.g., Khan et al., 1985; Pi et al., 1993; Zhang et al., 2000; Lynn et al., 2014; Chen et al. 2020, 2021; Wang et al., 2021). Based on these works, we explored the characteristics of DDMs using GPS VTEC data from a total of 537 GNSS tracking stations worldwide. The stations cover most of the world's land and parts of the ocean. Compared with previous studies, it can better reflect the characteristics of DDMs on a large scale. We found some interesting features in the global DDM phenomenon. For example, the occurrence rate of DDMs is quasi-symmetrical about the magnetic equator, the DDM phenomenon has obvious seasonal differences, and the occurrence time of DDMs in low latitudes is later than that in middle and high latitudes. Generally, the dynamic and photochemical processes act in concert to control the ionospheric variations. These processes are affected by many factors, such as solar irradiation, thermospheric composition and neutral winds, and ionospheric electric fields, which vary with seasons (Wang et al., 2021). Zhang et al. (2000) and Wang et al. (2021) pointed out that ionospheric DDMs are more likely to occur under lower background electron density/TEC conditions. This is entirely consistent with what we observed in the magnetic latitude range of −45°~45°, where there is a significant negative correlation between the occurrence rate of DDMs and background VTEC in this region. However, in the magnetic latitude range of 45°~70° in the northern hemisphere, the occurrence rate of DDMs seems to increase with the increase of background VTEC. Yu et al. (2006) pointed out that the contours of TEC annual amplitude seem to be parallel to the magnetic latitude. The annual amplitudes are smaller in the equatorial and low latitudes, while they are much larger at the high latitudes in both hemispheres, especially in northern Europe and southeastern Australia (Yu et al., 2006). This may be related to the higher occurrence rate of DDMs in Europe and a lower occurrence rate in low latitudes. Therefore, we suggest that the background TEC is still a precondition for the occurrence of the DDM phenomenon in ionospheric TEC, but the relationship between them may not be a negative correlation. In addition, the occurrence rate of DDMs showed significant hemispheric, seasonal, and regional differences. Some studies have shown that the dominant factors (equatorial electric field, thermospheric composition, neutral winds, etc.) that modulate the dynamic and photochemical processes may cause the hemispheric asymmetry of the TEC variations (Rishbeth, 1998; Yu et al., 2006; Adebiyi et al., 2020; Wang et al., 2021). Since solar irradiation modulates atmospheric circulation, the thermospheric composition (O/N_2) also depends on the season (Rishbeth, 1998). The low background electron density in summer is related to the low thermospheric composition O/N_2 ratio (Zhang et al., 2000; Wang et al., 2021), and the reduction of O/N_2 is more favorable for the formation of DDMs (Chen et al., 2021). We also observed that the occurrence rate of DDMs exhibits a quasi-symmetrical distribution on both sides of the magnetic equator, and the annual amplitude of O/N_2 also exhibits a symmetrical distribution with magnetic latitude (Yu et al., 2006). Therefore, the O/N_2 effect may play an important role in forming ionospheric DDMs. This may be an important reason for these differences in DDMs.

Furthermore, by observing the occurrence time of the DDM structures, we found that it has obvious latitude differences. The DDM phenomenon in mid/high latitudes usually occurs earlier than in low latitudes, which may be caused by poleward/equatorward neutral winds. Generally, vertical plasma drifts due to electromagnetic forces, meridional neutral winds, changes in chemical composition, or a combination of these are considered to be important factors causing DDMs (Katamzi et al., 2016). Kohl et al. (1968), Khan et al. (1985), Pi et al. (1993), and Katamzi et al. (2016) argued that the DDM phenomenon is caused by poleward/equatorward neutral winds rather than vertical $E \times B$ drifts. Since the tracking stations are located outside the equatorial anomaly region, and the

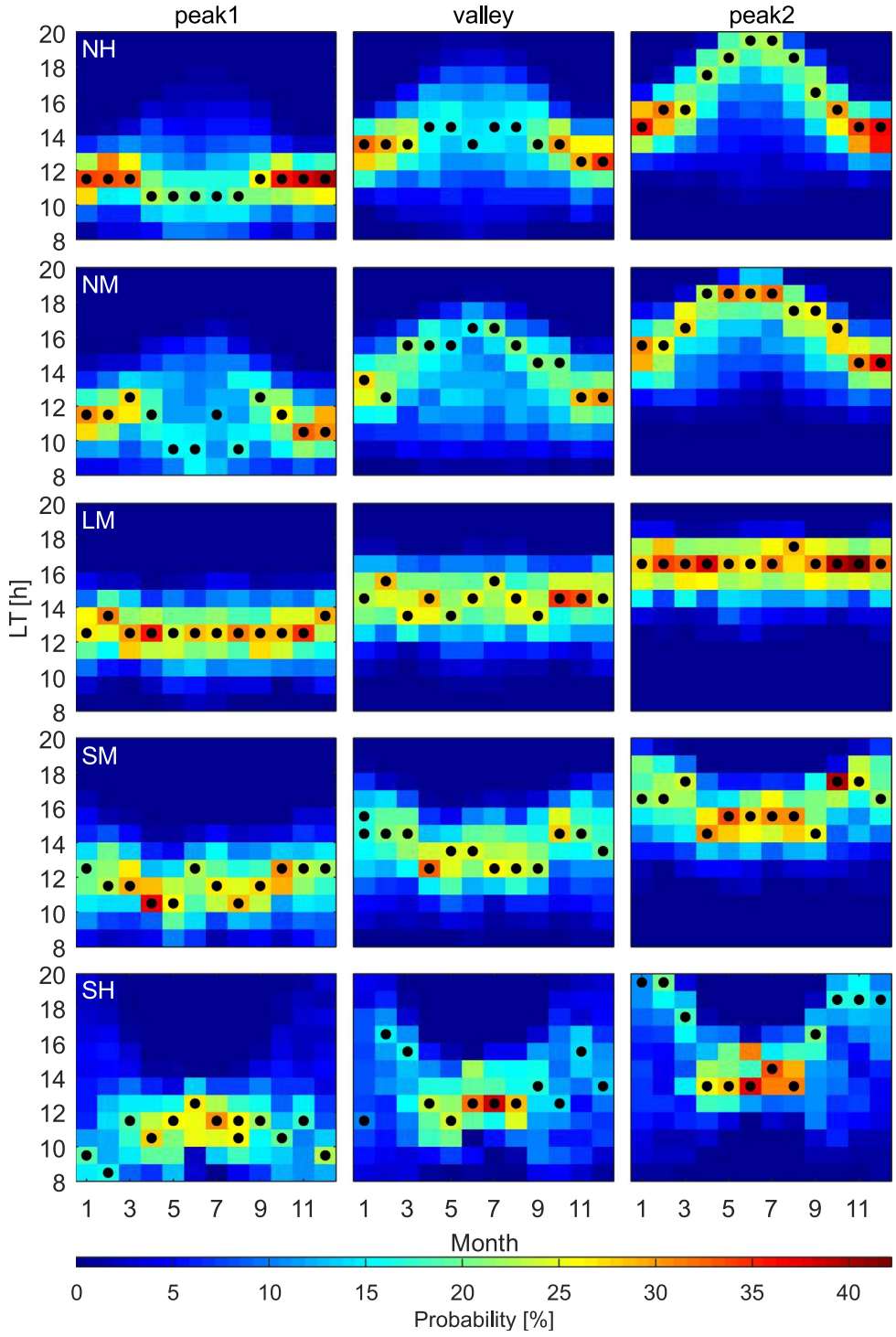

Figure 11. The occurrence time of the DDM structures in each month in different MLAT regions worldwide. Each row in the figure represents an MLAT region, and the black circles represent that the ionospheric DDMs have the highest occurrence rate in this period.

DDM structures mainly tend to propagate toward the equator, the DDM phenomenon does not originate from the enhancement of the equatorial eastward/westward electric field (Katamzi et al., 2016). Instead, the poleward/equatorward meridional winds were responsible for the DDMs because the equatorward (poleward) wind pushes the ionized plasma up (down) the magnetic field lines from higher (lower) to lower (higher) latitudes and from low (high)-loss region into a high (low)-loss region (Khan et al., 1985; Katamzi et al., 2016). Peak2 in the middle and high latitudes appears later in the local summer and earlier in the winter, which may be due to the longer sunshine time in summer, so peak2 tends to occur later.

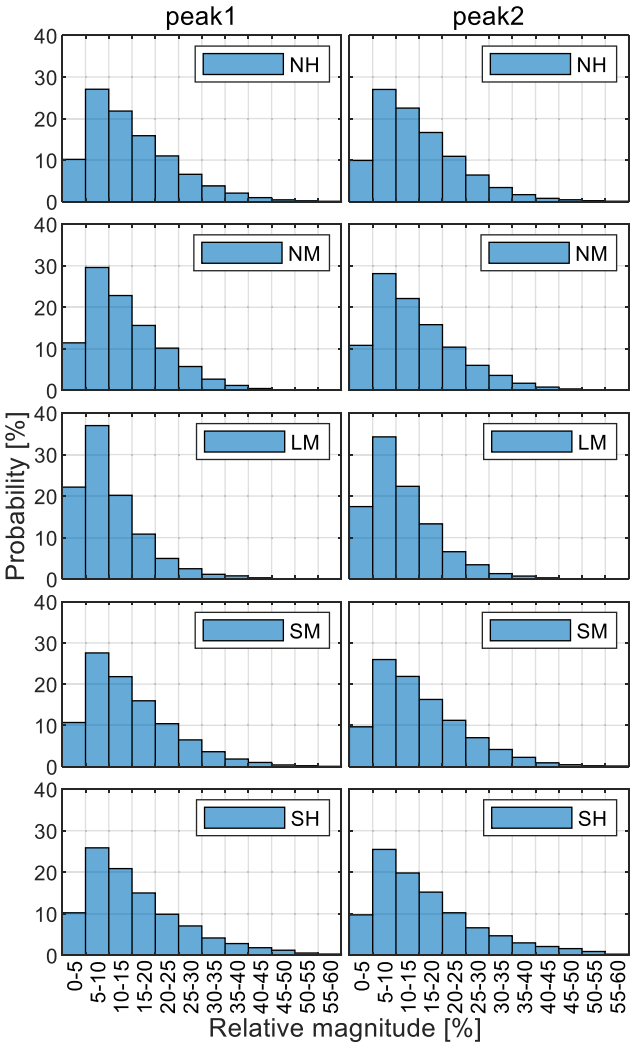

Figure 12. The probability distribution of the relative magnitude of the two peaks in different MLAT regions.

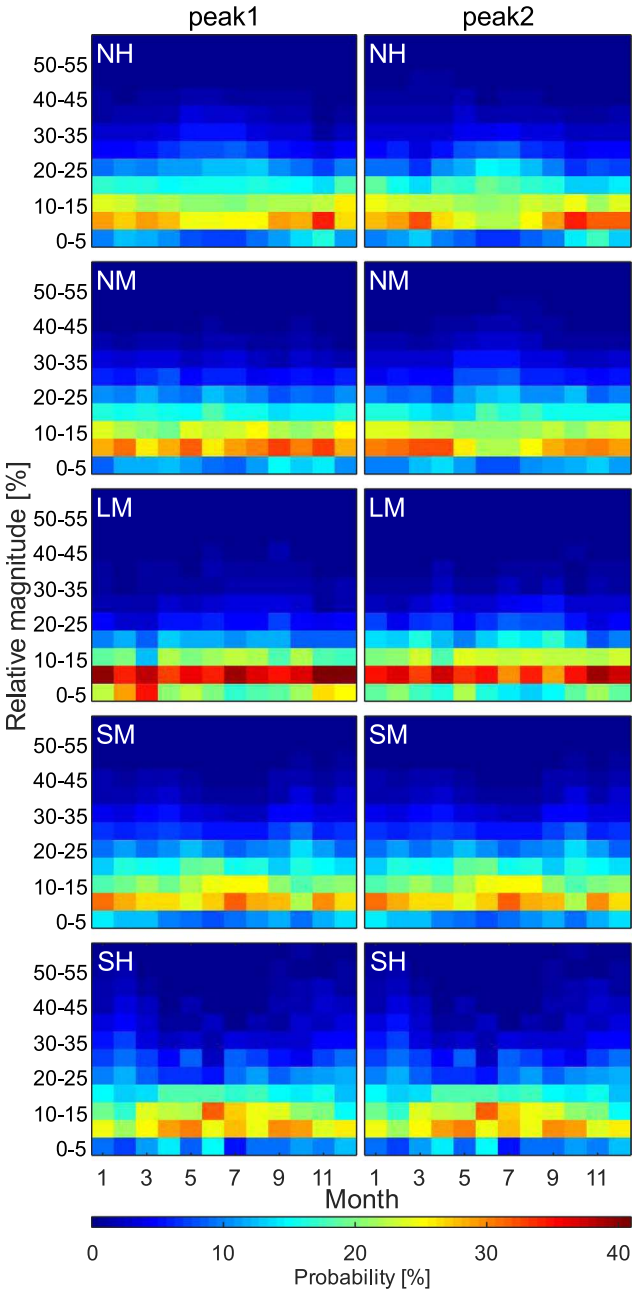

Figure 13. The probability distribution of the relative magnitude of the two peaks in different MLAT regions in each month.

The relative magnitude of DDMs reflects the enhancement/bite-out degree to a certain extent. The enhancement/bite-out degree in the middle and high latitudes is significantly higher than that in the low latitudes (see Fig. 12), which is similar to the result reported by Chen et al. (2021). Chen et al. (2021) pointed out that with the increase in latitude, DDMs became more obvious, and the degree of bite-out was also related to the diurnal variation magnitude of photoionization. If the diurnal variation magnitude of photoionization is smaller, the bite-out degree tends to be more significant. The variations of thermospheric composition and the upward diffusion outflow can more easily dominate over the enhancement of photoionization in the morning to form DDMs at higher latitudes (Chen et al., 2021). Seasonal differences in relative magnitude may also be related to this. Furthermore, in the longitude difference of DDM type, neutral wind, electric field, and neutral atmosphere seem to play an important role. Anderson (1973) pointed out that it is difficult to explain the longitude dependence of DDMs by neutral wind alone and suggested that the electric field and the increase in the vibrational temperature of N_2 have a non-negligible contribution to it. At present, there are relatively few studies on the longitude difference of DDMs, and more in-depth research is needed. Furthermore, the DDM characteristics observed with different data (e.g., TEC, foF2, etc.) still need further exploration.

5 Conclusions

This paper uses GPS observations from 537 GNSS tracking stations from 2019 to 2020 to study the ionospheric DDM phenomenon on a global scale. The characteristics of the DDM phenomenon are studied from four aspects, and the following conclusions are obtained:

Occurrence rate: The occurrence rate of DDMs shows obvious regional differences, latitudinal differences, longitudinal differences, and seasonal differences. The occurrence rate of DDMs in Europe, eastern North America, Greenland, and the eastern Antarctic is significantly higher than that in other regions, while the occurrence rate near the magnetic equator is significantly lower than that in other regions. The occurrence rate of DDMs is roughly quasi-symmetrical about the magnetic equator. In the northern hemisphere, as the MLAT increases, it first increases, then decreases, and finally increases. However, in the southern hemisphere, the trend is reversed, i.e., as MLAT decreases, it first increases, then decreases, and finally increases. The DDM phenomenon mainly occurs in May–August (summer in the northern hemisphere, winter in the southern hemisphere), but there are still obvious differences in the occurrence rate of different months in different regions.

Comparison of the magnitude of the DDM's two peaks: The DDM phenomenon is mainly manifested as the front peak significant type or the posterior peak significant type. The probability of front peak significant type shows an "M"-shaped variation with increasing longitude in the NH and NM (peaks near 120°W and 60°E), while there is no significant variation in the LM and SM, and an inverted "V"-shaped distribution in the range of 180°W–60°W in the SH (peaks near 140°W). The probabilities of the posterior peak significant type show the opposite trend with the increase of longitude in each region.

The occurrence time and duration of DDM structures: The occurrence time of DDM structures in each period shows obvious latitudinal and seasonal differences. The peak probability of the occurrence time of DDM structures in LM is delayed by about 1 h compared with other regions, and the duration is usually shorter than that in other regions. The duration of the DDM structures in the NM, LM, and SM is mainly concentrated in 3–4 h, while in the NH and SH, the duration is mainly concentrated in 2–4 h. Valley and peak2 in the NH, NM, SM, and SH occur earlier in the local winter than in the local summer, while the occurrence time of the DDM structures in the LM does not change much with the seasons.

The relative magnitude of the DDM's two peaks: The relative magnitudes of DDM's two peaks have latitudinal and seasonal differences. The relative magnitude of the two peaks in the LM is usually smaller, mainly concentrated in 0–15%, while in other regions, it is mainly concentrated in 5–20%. In the northern/southern hemisphere, as the latitude decreases/increases (getting closer to the equator), the relative magnitude of each peak has a gradually increasing trend in the probability within its main distribution range. The relative magnitude of the two peaks in each MLAT region has a certain seasonal difference in the probability within its peak range (5–10%). The relative magnitude of peak1 in the LM has a higher probability in November–January, March, and July. The relative magnitude of peak2 in the NH/NM has a lower probability in local summer.

Acknowledgements. The authors thank the CODE (Centre for Orbit Determination in Europe) for providing the GIMs (Global Ionospheric Maps), precision ephemeris, and DCBs (Differential Code Bias) products. The authors thank the IONOLAB Group for providing the IONOLAB-TEC software. The authors thank the Instituto Brasileiro de Geografia e Estatística (IBGE) for providing GPS observables for Brazil. The authors thank the IGS (International GNSS Service) and MGEX (Multi-GNSS Experiment) for providing the multi-GNSS observations. Finally, the authors thank the UNAVCO for providing the remaining GPS observations. This work was supported in part by the National Natural Science Foundation of China under Grant 41404031, in part by the State Key Laboratory of Geodesy and Earth's Dynamics, Innovation Academy for Precision Measurement Science and Technology under Grant SKLGED2022-3-5, in part by Beijing Key Laboratory of Urban Spatial Information Engineering under Grant 20210206, and in part by the Outstanding Youth Science Fund of Xi'an University of Science and Technology under Grant 2018YQ2-10. The IGS MGEX multi-GNSS observations used in the paper are public and can be accessed from the cddis website https://cddis.nasa.gov/archive/gnss/data/campaign/mgex/. The GPS observations in Brazil can be obtained via the website https://www.ibge.gov.br/geociencias/downloads-geociencias.html. Other GPS observations can be obtained via the website https://data.unavco.org/archive/gnss/rinex/obs/. The GIMs, precision ephemeris, and DCBs products can be obtained via the website https://www.aiub.unibe.ch/download/. Thanks to the editors and reviewers for their valuable comments. The editor thanks two anonymous reviewers for their assistance in evaluating this paper.

References

Anderson DN. 1973. A theoretical study of the ionospheric F region equatorial anomaly – II. Results in the American and Asian sectors. *Planet Space Sci* **21(3)**: 421–442. https://doi.org/10.1016/0032-0633(73)90041-X.

Adeniyi JO, Joshua BW. 2014. Latitudinal effect on the diurnal variation of the F2 layer at low solar activity. *J Atmos Sol Terr Phys* **120**: 102–110. https://doi.org/10.1016/j.jastp.2014.09.005.

Arikan FEZA, Erol CB, Arikan O. 2003. Regularized estimation of vertical total electron content from global positioning system data. *J Geophys Res Space Phys* **108(A12)**: https://doi.org/10.1029/2002JA009605.

Arikan FEZA, Erol CB, Arikan O. 2004. Regularized estimation of vertical total electron content from GPS data for a desired time period. *Radio Sci* **39(6)**: https://doi.org/10.1029/2004RS003061.

Arikan F, Arikan O, Erol CB. 2007. Regularized estimation of TEC from GPS data for certain midlatitude stations and comparison with the IRI model. *Adv Space Res* **39(5)**: 867–874. https://doi.org/10.1016/j.asr.2007.01.082.

Arikan FEZA, Nayir H, Sezen UMUT, Arikan O. 2008. Estimation of single station interfrequency receiver bias using GPS-TEC. *Radio Sci* **43(4)**: https://doi.org/10.1029/2007RS003785.

Adebesin BO, Rabiu AB, Obrou OK, Adeniyi JO. 2018. Ionospheric peak electron density and performance evaluation of IRI-CCIR near magnetic equator in Africa during two extreme solar activities. *Space Weather* **16(3)**: 230–244. https://doi.org/10.1002/2017SW001729.

Adebiyi S, Adimula I, Oladipo O. 2020. Inter-hemispheric comparison of ionospheric TEC variation at each latitudinal band during quiet geomagnetic condition. *J Niger Soc Phys Sci* 77–90. https://doi.org/10.46481/jnsps.2020.23.

Bhuyan PK, Borah RR. 2007. TEC derived from GPS network in India and comparison with the IRI. *Adv Space Res* **39(5)**: 830–840. https://doi.org/10.1016/j.asr.2007.01.082.

Chen Y, Liu L, Le H, Zhang H. 2020. Equatorial north-south difference of noontime electron density bite-out in the F2 layer. *J Geophys Res Space Phys* **125(8)**: e2020JA028124. https://doi.org/10.1029/2020JA028124.

Chen Y, Liu L, Le H, Zhang H. 2021. Latitudinal dependence of daytime electron density bite-out in the ionospheric F2-layer. *J Geophys Res Space Phys* **126(1)**: e2020JA028277. https://doi.org/10.1029/2020JA028277.

Erol CB, Arikan F, Arikan O. June 2002. A new technique for TEC estimation. In: *IEEE International Geoscience and Remote Sensing Symposium*, vol. **2**, pp. 1284–1286. https://doi.org/10.1109/IGARSS.2002.1025915.

Horvath I, Essex EA. 2003. The southern-hemisphere mid-latitude day-time and night-time trough at low-sunspot numbers. *J Atmos Sol Terr Phys* **65(8)**: 917–940. https://doi.org/10.1016/S1364-6826(03)00113-5.

Huang YN, Jeng BS. 1978. On the forenoon bite-out in the critical frequency of the F2-layer. *J Atmos Terr Phys* **40**: 581–584. https://doi.org/10.1016/0021-9169(78)90097-1.

Huang F, Li Q, Shen X, Xiong C, Yan R, Zhang SR, Wang W, Aa E, Zhong J, Dang T, Lei J. 2020. Ionospheric responses at low latitudes to the annular solar eclipse on 21 June 2020. *J Geophys Res Space Phys* **125(10)**: e2020JA028483. https://doi.org/10.1029/2020JA028483.

He S, Zhang D, Hao Y, Xiao Z. 2020. Statistical study on the occurrence of the ionospheric mid-latitude trough and the variation of trough minimum location over northern hemisphere. *Chinese J Geophys* **63(1)**: 31–46. https://doi.org/10.6038/cjg2020M0564.

Joshua BW, Adeniyi JO, Oladipo OA, Doherty PH, Adimula IA, Olawepo AO, Adebiyi SJ. 2018. Simultaneous response of NmF2 and GPS-TEC to storm events at Ilorin. *Adv Space Res* **61(12)**: 2904–2913. https://doi.org/10.1016/j.asr.2018.03.031.

Jonah OF, Goncharenko L, Erickson PJ, Zhang S, Coster A, Chau JL, Rideout W. 2020. Anomalous behavior of the equatorial ionization anomaly during the 2 July 2019 solar eclipse. *J Geophys Res Space Phys* **125(9)**: e2020JA027909. https://doi.org/10.1029/2020JA027909.

Katamzi Z. 2011. *Statistical analysis of ionospheric total electron content*. University of Bath, (Doctoral dissertation). https://researchportal.bath.ac.uk/en/studentTheses/statistical-analysis-of-ionospheric-total-electron-content.

Kohl H, King JW, Eccles D. 1968. Some effects of neutral air winds on the ionospheric F-layer. *J Atmos Terr Phys* **30(10)**: 1733–1744. https://doi.org/10.1016/0021-9169(68)90094-9.

Khan ZM, Ara H, Iqbal S, Nasir M. 1985. On the cause of fore-noon & post-noon bite-outs in foF2. *J Atmos Terr Phys* **47**: 719–724. https://doi.org/10.1016/0021-9169(85)90107-2.

Katamzi ZT, Smith ND, Mitchell CN, Spalla P. 2012. Analysis of diurnal double maxima observed above Italy during 1975–1991. *J. Atmos. Sol. Terr. Phys.* **89**: 67–75. https://doi.org/10.1016/j.jastp.2012.08.001.

Katamzi ZT, Habarulema JB, Giday NM. 2016. Daytime twin-peak structures observed at southern African and European middle latitudes on 8–13 April 2012. *Ann Geophys* **34**: 581–590. https://doi.org/10.5194/angeo-34-581-2016.

Karpachev AT, Klimenko MV, Klimenko VV. 2019. Longitudinal variations of the ionospheric trough position. *Adv Space Res* **63(2)**: 950–966. https://doi.org/10.1016/j.asr.2018.09.038.

Lee CC. 2012. Examination of the absence of noontime bite-out in equatorial total electron content. *J Geophys Res Space Phys* **117(A9)**: https://doi.org/10.1029/2012JA017909.

Lynn KJ, Gardiner-Garden RS, Heitmann A. 2014. The spatial and temporal structure of twin peaks and midday bite out in foF2 (with associated height changes) in the Australian and South Pacific low midlatitude ionosphere. *J Geophys Res Space Phys* **119(12)**: 10–294. https://doi.org/10.1002/2014JA020617.

Liu YW, Xu JS, Xu L, Yin F. 2015. A study on the position variation of mid-latitude ionospheric trough minimum and its controlling factors. *Chinese J Geophys* **58(1)**: 12–19. https://doi.org/10.6038/cjg20150102.

Moffett RJ, Quegan S. 1983. The mid-latitude trough in the electron concentration of the ionospheric F-layer: a review of observations and modelling. *J Atmos Terr Phy* **45(5)**: 315–343. https://doi.org/10.1016/S0021-9169(83)80038-5.

Mukherjee S, Sarkar S, Purohit PK, Gwal AK. 2010. Seasonal variation of total electron content at crest of equatorial anomaly station during low solar activity conditions. *Adv Space Res* **46(3)**: 291–295. https://doi.org/10.1016/j.asr.2010.03.024.

Nayir H, Arikan FEZA, Arikan O, Erol CB. 2007. Total electron content estimation with Reg-Est.. *J Geophy Res Space Phys* **112(A11)**: https://doi.org/10.1029/2007JA012459.

Ouattara F, Zoundi C, Fleury R. 2012. Comparison between CODG TEC and GPS based TEC observations at Koudougou station in Burkina Faso. *Indian J Radio Space Phys* **41**: 617–623. https://hal.archives-ouvertes.fr/hal-00940398.

Opio P, D'ujanga, FM, Ssenyonga T. 2015. Latitudinal variation of the ionosphere in the African sector using GPS TEC data. *Adv Space Res* **55(6)**: 1640–1650. https://doi.org/10.1016/j.asr.2014.12.036.

Oluwadare TS, Thai CN, Akala AOO, Heise S, Alizadeh M, Schuh H. 2019. Characterization of GPS-TEC over African equatorial ionization anomaly (EIA) region during 2009–2016. *Adv Space Res* **63(1)**: 282–301. https://doi.org/10.1016/j.asr.2018.08.044.

Pi X, Mendillo M, Fox MW, Anderson DN. 1993. Diurnal double maxima patterns in the F region ionosphere: Substorm-related aspects. *J Geophys Res Space Phys* **98(A8)**: 13677–13691. https://doi.org/10.1029/93JA00502.

Pryse SE, Kersley L, Williams MJ, Walker IK. 1998. The spatial structure of the dayside ionospheric trough. *Ann Geophys* **16**: 1169–1179. https://doi.org/10.1007/s00585-998-1169-4.

Pavan Chaitanya P, Patra AK, Balan N, Rao SVB. 2015. Ionospheric variations over Indian low latitudes close to the equator and comparison with IRI-2012. *Ann Geophys* **33**: 997–1006. https://doi.org/10.5194/angeo-33-997-2015.

Rajaram G. 1977. Structure of the equatorial F-region, topside and bottomside – A review. *J Atmos Terr Phys* **39(9–10)**: 1125–1144. https://doi.org/10.1016/0021-9169(77)90021-6.

Rishbeth H. 1998. How the thermospheric circulation affects the ionospheric F2-layer. *J Atmos Sol Terr Phys* **60(14)**: 1385–1402. https://doi.org/10.1016/S1364-6826(98)00062-5.

Saryo T, Takeda M, Araki T, Sato T, Tsuda T, Fukao S, Kato S. 1989. A midday bite-out event of the F2-layer observed by MU radar. *J Geomagn Geoelectr* **41(8)**: 727–734. https://doi.org/10.5636/jgg.41.727.

Sezen UMUT, Arikan FEZA, Arikan O, Ugurlu O, Sadeghimorad A. 2013. Online, automatic, near-real time estimation of GPS-TEC: IONOLAB-TEC. *Space Weather* **11(5)**: 297–305. https://doi.org/10.1002/swe.20054.

Venkatesh K, Fagundes PR, de Abreu AJ, Pillat VG. 2016. Unusual noon-time bite-outs in the ionospheric electron density around the anomaly crest locations over the Indian and Brazilian sectors during quiet conditions – A case study. *J Atmos Sol Terr Phys* **147**: 126–137. https://doi.org/10.1016/j.jastp.2016.07.016.

Wang Y, Huang F, Lei J, Luan X, Dou X. 2021. Ionospheric diurnal double-maxima patterns observed by the TEC from Beidou

Geostationary Satellites in the Asian-Australian Sector during 2016–2018. *J Geophys Res Space Phys* **126(1)**: e2020JA028578. https://doi.org/10.1029/2020JA028578.

Wang R, Chen P, Yao Y, An Z, Wang Z. 2022. Research on the ionospheric diurnal double-maxima patterns in Asia-Australian area based on the VTEC observations of BDS geostationary satellites. *Adv Space Res* **69(10)**: 3705–3716. https://doi.org/10.1016/j.asr.2022.02.041.

Yu T, Wan WX, Liu LB, Tang W, Luan XL, Yang GL. 2006. Analysis of global TEC annual and semi-annual variations by using IGS data. *Chinese J Geophys* **49(4)**: 841–847. https://doi.org/10.1002/cjg2.903.

Yang N, Le H, Liu L. 2015. Statistical analysis of ionospheric mid-latitude trough over the Northern Hemisphere derived from GPS total electron content data. *Earth Planets Space* **67(1)**: 1–11. https://doi.org/10.1186/s40623-015-0365-1.

Zhang SR, Oliver WL, Fukao S, Otsuka Y. 2000. A study of the forenoon ionospheric F2 layer behavior over the middle and upper atmospheric radar. *J Geophys Res Space Phys* **105(A7)**: 15823–15833. https://doi.org/10.1029/2000JA000007.

Cite this article as: Chen P, Wang R, Yao Y, An Z & Wang Z, et al. 2022. On the global ionospheric diurnal double maxima based on GPS vertical total electron content. *J. Space Weather Space Clim.* **12**, 38. https://doi.org/10.1051/swsc/2022035.